New One-Dimensional Vanadyl Iodates: Hydrothermal Preparation, Structures, and NLO Properties of $A[VO_2(IO_3)_2]$ (A = K, Rb) and $A[(VO)_2(IO_3)_3O_2]$ (A = NH_4, Rb, Cs)

Richard E. Sykora,[†] Kang Min Ok,[‡] P. Shiv Halasyamani,[‡] Daniel M. Wells,[†] and Thomas E. Albrecht-Schmitt*,[†]

Department of Chemistry, Auburn University, Auburn, Alabama 36849, and Department of Chemistry, University of Houston, Houston, Texas 77204-5003

Received January 14, 2002. Revised Manuscript Received April 8, 2002

Under mild hydrothermal conditions V_2O_5 reacts with AIO_4 (A = NH_4, K, Rb, Cs) and I_2O_5 to yield $A[VO_2(IO_3)_2]$ (K (**1**), Rb (**2**)) and $A[(VO)_2(IO_3)_3O_2]$ (A = NH_4 (**3**), Rb (**4**), Cs (**5**)) in the form of yellow to dark orange crystals. While **1** and **2** are not isostructural, both contain one-dimensional $^1_\infty[VO_2(IO_3)_2]^{1-}$ chains separated by K^+ or Rb^+ cations. These chains are constructed from five-coordinate V(V) atoms that are bound by two terminal oxo atoms to create a *cis*-VO_2^+ moiety and by one monodentate and two bridging iodate anions to create a distorted square pyramidal geometry. Compounds **3**−**5** are isostructural and contain orthorhombically distorted, octahedral V(V) with a single terminal oxo ligand. In addition, each vanadium center forms bonds with two bridging oxo atoms that are trans to one another and three bridging iodate anions in a mer arrangement. The bridging of the vanadium atoms by the oxo and iodate anions creates zigzagging one-dimensional $^1_\infty[(VO)_2(IO_3)_3O_2]^{1-}$ chains that are separated from one another by NH_4^+, Rb^+, or Cs^+ cations that reside in asymmetric environments. Compounds **3**−**5** crystallize in the polar space group *Ima*2. The polarity in these structures is imparted by the alignment of the stereochemically active lone pairs of electrons of the iodate anions along the *c*-axis. Second-harmonic generation measurements on **5** show a large response of 500× α-quartz.

Introduction

The hydrothermal behavior of vanadium typifies our concepts of chemical and structural flexibility in extended solids. Interest in vanadium-based materials stems from their ability to act as intercalation,[1−7] ion-exchange,[8] sorption,[8] magnetic,[9−13] and cathode[14−16] materials and as selective oxidation catalysts.[17−21] For example, $V_2O_5 \cdot nH_2O$ porous xerogels can be intercalated with numerous organic molecules, alkali metals, and transition metal complexes.[2,22−26] When thiophene, aniline, and other organic amines are intercalated into these xerogels, the V(V) becomes partially reduced to V(IV) with concomitant oxidation of the organic substrate. The resultant mixed-valent compounds display properties comparable to alkali metal bronzes obtained from high-temperature solid-state reactions.[12,27] In a

* To whom correspondence should be addressed.
[†] Auburn University.
[‡] University of Houston.

(1) Whittingham, M. S.; Jacobson, A. J. *Intercalation Chemistry*; Academic Press: New York, 1982.
(2) Lemordant, D.; Bouhaouss, A.; Aldebert, P.; Baffier, N. *Mater. Res. Bull.* **1986**, *21*, 273.
(3) Jacobson, A. J.; Johnson, J. W. *Angew. Chem., Int. Ed. Engl.* **1983**, *22*, 412.
(4) Jacobson, A. J.; Johnson, J. W.; Brody, J. F.; Scanlon, J. C.; Lewandowski, J. T. *Inorg. Chem.* **1985**, *24*, 1782.
(5) Lii, K. H. *J. Chin. Chem. Soc.* **1992**, *39*, 569.
(6) Wang, S. L.; Kang, H. Y.; Cheng, C. Y.; Lii, K. H. *Inorg. Chem.* **1991**, *30*, 3496.
(7) Kang, H. Y.; Lee, W. C.; Wang, S. L.; Lii, K. H. *Inorg. Chem.* **1992**, *31*, 4743.
(8) Khan, M. I.; Meyer, L. M.; Haushalter, R. C.; Schweitzer, A. L.; Zubieta, J.; Dye, J. L. *Chem. Mater.* **1996**, *8*, 43.
(9) Papoutsakis, D.; Jackson, J. E.; Nocera, D. G. *Inorg. Chem.* **1996**, *35*, 800.
(10) Bideau, J. L.; Papoutsakis, D.; Jackson, J. E.; Nocera, D. G. *J. Am. Chem. Soc.* **1997**, *119*, 1313.
(11) Plass, W. *Angew. Chem., Int. Ed. Engl.* **1996**, *35*, 627.
(12) Zhang, Y.; Warren, C. J.; Haushalter, R. C. *Chem. Mater.* **1998**, *10*, 1059.
(13) Kodama, K.; Harashima, H.; Sasaki, H.; Kobayashi, Y.; Kasi, M.; Taniguchi, S.; Yasui, Y.; Sato, M.; Kakurai, K.; Mori, T.; Nishi, M. *J. Phys. Soc. Jpn.* **1997**, *66*, 793.
(14) Whittingham, M. S.; Chianelli, R. R.; Jacobson, A. J. *Proc. Electrochem. Soc.* **1980**, *80*, 206.
(15) Whittingham, M. S. *Mater. Res. Bull.* **1978**, *13*, 959.
(16) Folkesson, B. *J. Appl. Electrochem.* **1990**, *20*, 907.
(17) Centi, G.; Trefiro, F.; Ebner, J. R.; Franchetti, V. M. *Chem. Rev.* **1988**, *88*, 55.
(18) Sleight, A. W. *Catal. Today* **1987**, *1*, 347.
(19) Bordes, E. *Catal. Today* **1987**, *1*, 499.
(20) Horowitz, H. S.; Blackstone, C. M.; Sleight, A. W.; Teufer, G. *Appl. Catal.* **1988**, *38*, 193.
(21) Guiliants, V. V.; Benziger, J. B.; Sundaresan, S. *Catalysis* **1996**, *101*, 991.
(22) Paul-Boucour, V.; Aldebert, P. *Mater. Res. Bull.* **1983**, *18*, 1247.
(23) Lemordant, D.; Bouhaouss, A.; Aldebert, P.; Baffier, N. *J. Chim. Phys. Phys.-Chim. Biol.* **1986**, *83*, 105.
(24) Ruiz-Hitzky, E.; Casal, B. *J. Chem. Soc., Faraday Trans. 1* **1986**, *82*, 1597.
(25) Hasbah, H.; Tinet, D.; Crespin, M. M.; Erre, R.; Setton, R.; Van Damme, H. *J. Chem. Soc., Chem. Commun.* **1985**, 935.
(26) Kanatzidis, M.; Marks, T. J. *Inorg. Chem.* **1987**, *26*, 783.
(27) Hagenmuller, P. In *Non-Stoichiometric Compounds, Tungsten Bronzes, Vanadium Bronzes and Related Compounds*; Bevan, D. J., Hagenmuller, P., Eds.; Pergamon Press: Oxford, U.K., 1973; Vol. 1.

10.1021/cm020021n CCC: $22.00
Published on Web 05/15/2002

similar fashion, ion exchange in V(V) compounds often coincides with reduction of some or all of the vanadium to the tetravalent oxidation state. This is aptly illustrated by the layered vanadyl phosphate, $VOPO_4$, which undergoes reductive intercalation of alkali metals under hydrothermal conditions to yield the nonstoichiometric, ferromagnetic compounds, $A_{0.5}VOPO_4 \cdot 1.5H_2O$ (A = Na, K, Rb).[4,9] Likewise, when V_2O_5 is reacted with $CuCl_2 \cdot 2H_2O$ and ethylenediamine (en) under mild hydrothermal conditions, $[Cu(en)_2][V_6O_{14}]$ is isolated. This compound contains $Cu(en)_2^{2+}$ cations intercalated between mixed-valent $^2_\infty[V_6O_{14}]^{2-}$ sheets.[28]

As demonstrated by the aforementioned examples, vanadium oxides and phosphates are well-suited for the tailoring and enhancement of a variety of physicochemical properties. One recent method for achieving this goal is to prepare microporous vanadium-based materials. This has been accomplished with the preparation and structural characterization of the microporous vanadium phosphates, $[am]K_{1.35}[V_5O_9(PO_4)_2] \cdot nH_2O$ (am = DABCO ($C_6H_{14}N_2$) or piperidinium ($C_4H_{12}N_2$)), and $Cs_3[V_5O_9(PO_4)_2] \cdot nH_2O$.[8] These compounds undergo rapid ion-exchange reactions with Ba^{2+} and NH_4^+ and show the ability to absorb 10 wt % water.[8] Likewise, control of the magnetic properties of the layered vanadyl phosphonates, $VO(O_3PC_6H_4{-}X) \cdot nH_2O$ (X = *p*-NO_2, *m*-F, *p*-Cl, *p*-F, H, *p*-CH_3), has also been achieved through the sequential modification of the electronic environment of the phosphorus atoms.[10]

Finally, the production and catalytic behavior of several vanadium phosphates has been intensely investigated based on their ability to act as selective oxidation catalysts as in the oxidation of butane to maleic anhydride by $(VO)_2P_2O_7$.[17−21] Interest in these catalysts has inspired several studies on the preparation of low-dimensional and open-framework vanadium phosphates that can either serve as catalysts in their own right or be thermally decomposed to known catalysts in the form of high surface area solids. A recent report by Jacobson and co-workers demonstrated that the vanadyl oxalatophosphates, $[C_2H_{10}N_2][VO(HPO_4)]_2(C_2O_4)$ and $[CH_6N_3]_2[VO(HPO_4)]_2(C_2O_4)$, undergo thermal decomposition above ≈550 °C to yield porous, crystalline powders of $(VO)_2P_2O_7$.[29]

The ability of vanadium to function in such vastly different manners is made possible by its structural versatility since it has been observed in three-, four-, five-, and six-coordinate environments. Furthermore, vanadium also has readily accessible oxidation states from II−V. However, the majority of compounds derived from hydrothermal conditions display tetrahedral, trigonal bipyramidal, square pyramidal, or octahedral coordination in either the tetra- or pentavalent oxidation states. Many compounds contain multiple coordination environments for vanadium, and mixed-valent systems are common. For example, the layered vanadium oxides, α-, β-$[H_3N(CH_2)_2NH_3][V_4O_{10}]$ and α-, β-$[H_2N(C_2H_4)_2NH_2)][V_4O_{10}]$, contain $V^{5+}O_4$ tetrahedra and $V^{4+}O_5$ square pyramids.[30] The microporous structures of $[am]K_{1.35}[V_5O_9(PO_4)_2] \cdot nH_2O$ (am = DABCO ($C_6H_{14}N_2$) or piperidinium ($C_4H_{12}N_2$)) and $Cs_3[V_5O_9(PO_4)_2] \cdot nH_2O$ are also constructured from tetrahedral V(V) and square pyramidal V(IV).[8]

Our interest in vanadium is based on its ability to form a vanadyl, *cis*-VO_2^+, moiety in acidic aqueous media. When four additional ligands bind the vanadyl moiety, the resultant geometry is forced from being an idealized octahedron because of the bent nature of the O=V=O bond angle (≈107°) and the potential for a second-order Jahn−Teller distortion.[31−39] This type of distortion is prevalent in high-valent, d^0 transition metals owing to the symmetry-allowed mixing of a low-lying excited state (LUMO) with a nondegenerate ground-state molecular orbital (HOMO).[31−39] This orbital mixing results in a distortion of the geometry of the metal centers along the C_2, C_3, or C_4 axes whose magnitude is partially a function of the charge of the metal center, with increasing charge resulting in a smaller HOMO−LUMO gap.[37−39] We have recently shown that by combining distorted MoO_6 octahedra with the C_{3v} iodate anion and a large counterion such as Rb^+ or Cs^+ that new polar solids with large second-harmonic generation (SHG) responses can be prepared.[40] Herein, we demonstrate that these same principles can be applied to the preparation of the new V(V) iodates, $A[VO_2(IO_3)_2]$ (K (**1**), Rb (**2**)) and $A[(VO)_2(IO_3)_3O_2]$ (A = NH_4 (**3**), Rb (**4**), Cs (**5**)). The latter compounds are polar, and the second-harmonic generation measurements of **5** are reported. Prior to this work, the only report on a structurally characterized vanadium iodate is that of $VO_2IO_3 \cdot 2H_2O$.[41]

Experimental Section

Syntheses. V_2O_5 (99.95%, Alfa-Aesar), Cs_2CO_3 (99%, Alfa-Aesar), Rb_2CO_3 (99%, Alfa-Aesar), $(NH_4)_2CO_3$ (99.7%, Matheson), H_5IO_6 (98%, Alfa-Aesar), I_2O_5 (98%, Alfa-Aesar), and KIO_4 (99.9%, Fisher) were used as received. NH_4IO_4, $RbIO_4$, and $CsIO_4$ were prepared from the reaction of $(NH_4)_2CO_3$, Rb_2CO_3, or Cs_2CO_3 with H_5IO_6 as reported by de Waal et al.[42] Distilled and Millipore-filtered water with a resistance of 18.2 MΩ was used in all reactions. Reactions were run using 1 mL of water in Parr 4749 23-mL autoclaves with PTFE liners for 6 days at 180 °C and cooled at a rate of 9 °C/h to 23 °C. The resultant mother liquors were decanted from crystalline products that were subsequently washed with methanol. SEM/EDX analyses were performed using a JEOL 840/Link Isis instrument.

(28) Ollivier, P. J.; DeBoard, J. R. D.; Zapf, P. J.; Zubieta, J.; Meyer, L. M.; Wang, C. C.; Mallouk, T. E.; Haushalter, R. C. *J. Mol. Struct.* **1998**, *470*, 49.
(29) Do, J.; Bontchev, R. P.; Jacobson, A. J. *Chem. Mater.* **2001**, *13*, 2601.
(30) Zhang, Y.; Haushalter, R. C.; Clearfield, A. *Inorg. Chem.* **1996**, *35*, 4950.
(31) Opik, U.; Pryce, M. H. L. *Proc. R. Soc.* (*London*) **1937**, *A161*, 220.
(32) Wheeler, R. A.; Whangbo, M. H.; Hughbanks, T.; Hoffman, R.; Burdett, J. K.; Albright, T. A. *J. Am. Chem. Soc.* **1986**, *108*, 2222.
(33) Pearson, R. G. *J. Mol. Struct.* **1983**, *103*, 25.
(34) Kang, S. K.; Tang, H.; Albright, T. A. *J. Am. Chem. Soc.* **1993**, *115*, 1971.
(35) Cohen, R. E. *Nature* **1992**, *358*, 136.
(36) Burdett, J. K. *Molecular Shapes*; Wiley-Interscience: New York, 1980.
(37) Kunz, M.; Brown, I. D. *J. Solid State Chem.* **1995**, *115*, 395.
(38) Goodenough, J. B.; Longo, J. M. Crystallographic and magnetic properties of perovskite and perovskite-related compounds. In *Landolt-Bornstein*; Hellwege, K. H., Hellwege, A. M., Eds.; Springer-Verlag: Berlin, 1970; Vol. 4, pp 126−314.
(39) Brown, I. D. *Acta Crystallogr.* **1977**, *B33*, 1305.
(40) Sykora, R. E.; Kang, M. O.; Halasyamani, P. S.; Albrecht-Schmitt, T. E. *J. Am. Chem. Soc.* **2002**, *124*, 1951.
(41) Meschede, W.; Mattes, R. *Z. Anorg. Allg. Chem.* **1976**, *420*, 25.
(42) de Waal, D.; Range, K.-J. *Z. Naturforsch.* **1996**, *51b*, 1365.

Table 1. Crystallographic Data for $K[VO_2(IO_3)_2]$ (1), $Rb[VO_2(IO_3)_2]$ (2), $NH_4[(VO)_2(IO_3)_3O_2]$ (3), $Rb[(VO)_2(IO_3)_3O_2]$ (4), and $Cs[(VO)_2(IO_3)_3O_2]$ (5)

	1	**2**	**3**	**4**	**5**
formula					
formula mass	471.84	518.21	708.63	776.05	823.49
space group	$P2_1/n$ (No. 14)	$P\bar{1}$ (No. 2)	$Ima2$ (No. 46)	$Ima2$ (No. 46)	$Ima2$ (No. 46)
a (Å)	9.400(2)	5.2878(9)	14.099(2)	14.121(1)	14.181(1)
b (Å)	5.2383(8)	7.983(1)	10.214(1)	10.2392(7)	10.3178(8)
c (Å)	15.725(3)	9.669(2)	8.051(1)	8.0300(6)	8.0756(7)
α (deg)	90	72.456(3)	90	90	90
β (deg)	104.799(3)	89.686(3)	90	90	90
γ (deg)	90	87.929(3)	90	90	90
V (Å^3)	748.6(2)	388.9(1)	1159.4(3)	1161.1(1)	1181.6(2)
Z	4	2	4	4	4
T (°C)	−80	−80	−80	−80	−80
λ (Å)	0.71073	0.71073	0.71073	0.71073	0.71073
ρ_{calcd} (g cm^{-3})	4.186	4.425	4.037	4.440	4.629
μ(Mo Kα) (cm^{-1})	101.36	154.38	96.72	138.19	125.23
$R(F)^a$	0.0259	0.0350	0.0353	0.0442	0.0302
$R_w(F_o^2)^b$	0.0853	0.0884	0.0823	0.1179	0.0851

^{a} $R(F) = \sum||F_o| - |F_c||/\sum|F_o|$. ^{b} $R_w(F_o^2) = [\sum[w(F_o^2 - F_c^2)^2]/\sum wF_o^4]^{1/2}$.

Typical results are within 4% of the ratios determined from single-crystal X-ray diffraction. IR spectra were collected on a Nicolet 5PC FT-IR spectrometer from KBr pellets.

$K[VO_2(IO_3)_2]$ (1). Compound **1** was prepared from the reaction of V_2O_5 (93 mg, 0.51 mmol), KIO_4 (236 mg, 1.02 mmol), and I_2O_5 (171 mg, 0.51 mmol). The product consisted of a colorless solution over small, bright yellow prisms of **1**. Yield, 321 mg (66% yield based on V). EDX analysis for $K[VO_2(IO_3)_2]$ provided a K:V:I ratio of 1:1:2. IR (KBr, cm^{-1}): ν(V═O, V−O, and I═O) 935 (m), 911 (s), 840 (m), 793 (s), 785 (m, sh), 765 (s), 725 (s, sh), 717 (s, sh), 690 (s, sh), 680 (s, sh), 519 (s), 464 (s), 441 (m, sh).

$Rb[VO_2(IO_3)_2]$ (2). Compound **2** was prepared from the reaction of V_2O_5 (85 mg, 0.47 mmol), $RbIO_4$ (259 mg, 0.94 mmol), and I_2O_5 (156 mg, 0.47 mmol). The product consisted of a colorless solution over small, yellow prisms of **2**. Yield, 322 mg (66% yield based on Rb). EDX analysis for $Rb[VO_2(IO_3)_2]$ provided a Rb:V:I ratio of 1:1:2. IR (KBr, cm^{-1}): ν(V═O, V−O, and I−O) 933 (s), 910 (s), 841 (s), 790 (s), 779 (s), 762 (s), 729 (s), 688 (br, s), 512 (m), 468 (s), 433 (m).

$NH_4[(VO)_2(IO_3)_3O_2]$ (3). Compound **3** was prepared from the reaction of V_2O_5 (97 mg, 0.54 mmol), NH_4IO_4 (224 mg, 1.07 mmol), and I_2O_5 (179 mg, 0.54 mmol). The product consisted of a colorless solution over orange-brown hexagonal blocks of **3**. Yield, 285 mg (75% yield based on V). EDX analysis for $NH_4[(VO)_2(IO_3)_3O_2]$ provided a V:I ratio of 2:3. IR (KBr, cm^{-1}): ν(N−H, V═O, V−O, and I−O) 3232 (s, br), 926 (s), 908 (s), 880 (w, sh), 862 (s), 845 (m), 832 (w, sh), 800 (s, br), 755 (s, br), 737 (s, sh), 720 (s), 683 (s), 619 (m, br).

$Rb[(VO)_2(IO_3)_3O_2]$ (4). Compound **4** was prepared from the reaction of V_2O_5 (115 mg, 0.63 mmol), $RbIO_4$ (174 mg, 0.63 mmol), and I_2O_5 (211 mg, 0.63 mmol). The product consisted of a colorless solution over yellow prisms of **2** (235 mg, 72%) and deep orange hexagonal blocks of **4**. Yield, 130 mg (27% yield based on V). EDX analysis for $Rb[(VO)_2(IO_3)_3O_2]$ provided a Rb:V:I ratio of 1:2:3. IR (KBr, cm^{-1}): ν(V═O, V−O, and I−O) 925 (m), 907 (m), 881 (w, sh), 865 (m), 838 (m), 802 (m, br), 758 (s, br), 740 (s, sh), 719 (s), 681 (s), 621 (m, br).

$Cs[(VO)_2(IO_3)_3O_2]$ (5). Compound **5** was prepared from the reaction of V_2O_5 (108 mg, 0.60 mmol), $CsIO_4$ (193 mg, 0.60 mmol), and I_2O_5 (199 mg, 0.60 mmol). The product consisted of a colorless solution over orange hexagonal blocks of **5**. Yield, 390 mg (80% yield based on V). EDX analysis for $Cs[(VO)_2(IO_3)_3O_2]$ provided a Cs:V:I ratio of 1:2:3. IR (KBr, cm^{-1}): ν(V═O, V−O, and I═O) 926 (s), 910 (m), 881 (w), 865 (m), 845 (w), 839 (w), 798 (m, br), 757 (m, br), 739 (m, sh), 720 (w, sh), 681 (m, br), 668 (w, br), 620 (m, br).

Secord-Order NLO Measurements. Powder SHG measurements were performed on a modified Kurtz-NLO system using a 1064-nm light source.[43] A detailed description of the apparatus has been published.[44] Polycrystalline $Cs[(VO)_2(IO_3)_3O_2]$ (**5**) was ground and sieved into distinct particle size ranges, <20, 20−45, 45−63, 63−75, 75−90, and 90−125 μm. To make relevant comparisons with known SHG materials, crystalline SiO_2 and $LiNbO_3$ were also ground and sieved into the same particle size range. All of the powders were placed in separate capillary tubes. No index-matching fluid was used in any of the experiments. $I^{2\omega}/I^{2\omega}$ (SiO_2) is taken for a particle size range of 45−63 μm.

UV−Vis Diffuse Reflectance Spectra. Diffuse reflectance spectra for **1** and **5** were measured using a Shimadzu UV2501 spectrophotometer equipped with an integrating sphere attachment with $BaSO_4$ being used as the standard. The Kubelka-Monk function was used to convert diffuse reflectance data to absorbance spectra.[45]

Crystallographic Studies. Crystals of $K[VO_2(IO_3)_2]$ (**1**), $Rb[VO_2(IO_3)_2]$ (**2**), $NH_4[(VO)_2(IO_3)_3O_2]$ (**3**), $Rb[(VO)_2(IO_3)_3O_2]$ (**4**), and $Cs[(VO)_2(IO_3)_3O_2]$ (**5**) were mounted on glass fibers and aligned on a Bruker SMART APEX CCD X-ray diffractometer. Intensity measurements were performed using graphite monochromated Mo Kα radiation from a sealed tube with a monocapillary collimator. SMART was used for preliminary determination of the cell constants and data collection control. For all compounds, the intensities of reflections of a sphere were collected by a combination of three sets of exposures (frames). Each set had a different ϕ angle for the crystal and each exposure covered a range of 0.3° in ω. A total of 1800 frames were collected with an exposure time per frame of 30 s.

For **1**−**5**, determination of integral intensities and global cell refinement were performed with the Bruker SAINT (v 6.02) software package using a narrow-frame integration algorithm. A semiempirical absorption correction was applied based on the intensities of symmetry-related reflections measured at different angular settings using SADABS.[46] The program suite SHELXTL (v 5.1) was used for space group determination (XPREP), structure solution (XS), and refinement (XL).[47] The final refinements included anisotropic displacement parameters for all atoms and a secondary extinction parameter. Some crystallographic details are listed in Table 1 for **1**−**5**, additional details can be found in the Supporting Information.

(43) Kurtz, S. K.; Perry, T. T. *J. Appl. Phys.* **1968**, *39*, 3798.

(44) Porter, Y.; Ok, K. M.; Bhuvanesh, N. S. P.; Halasyamani, P. S. *Chem. Mater.* **2001**, *13*, 1910.

(45) Wendlandt, W. W.; Hecht, H. G. *Reflectance Spectroscopy*; Interscience Publishers: New York, 1966.

(46) *SADABS*. Program for absorption correction using SMART CCD based on the method of Blessing: Blessing, R. H. *Acta Crystallogr.* **1995**, *A51*, 33.

(47) Sheldrick, G. M. *SHELXTL PC*, Version 5.0, an Integrated System for Solving, Refining, and Displaying Crystal Structures from Diffraction Data; Siemens Analytical X-ray Instruments, Inc.: Madison, WI, 1994.

The absolute structure parameters of $NH_4[(VO)_2(IO_3)_3O_2]$ (**3**), $Rb[(VO)_2(IO_3)_3O_2]$ (**4**), and $Cs[(VO)_2(IO_3)_3O_2]$ (**5**) are 0.46(9), 0.00, and 0.16(8). This implies that most or all of the chains in **4** and **5** have the same direction of polar alignment. The crystal of **3** that was investigated, however, is a racemic twin. In **3**−**5** the thermal ellipsoids of the vanadium atoms show elongation along the *a*-axis. Because the ellipsoids for both lighter and heavier atoms in these structures are normal, this appears to be a real aspect of these structures and not an artifact caused by absorption or extinction. A probable explanation for this phenomenon is that there is a small distortion of the vanadium atoms along the C_4 axis of the VO_6 octahedra, which alternates back and forth as the chains propagate down the axis, that is, a Peierls distortion. Therefore, the vanadium site located in these structures is an average of two slightly displaced vanadium sites. Given the very close proximity of these sites, it is probably not reasonable to refine the vanadium atom as being disordered over these two sites. Furthermore, least-squares refinements do not suggest splitting the site to account for the elongation of the thermal ellipsoid along the chain axis.

Results and Discussion

Syntheses. The reaction of V_2O_5 with AIO_4 (A = NH_4, K, Rb, Cs) and I_2O_5 at 180 °C in aqueous media for 6 days produces $A[VO_2(IO_3)_2]$ (K (**1**), Rb (**2**)) and $A[(VO)_2(IO_3)_3O_2]$ (A = NH_4 (**3**), Rb (**4**), Cs (**5**)) in the form of yellow to dark orange crystals in yields ranging from 27 to 80%. Both reaction stoichiometry and cation size play important roles in the syntheses of these compounds. Furthermore, we have found that these reactions require unusually long durations to reach completion, and three-day reactions are far from adequate to isolate pure phases. The only redox chemistry that occurs in these syntheses is the reduction of the I(VII) in metaperiodate, IO_4^-, by water to I(V) in IO_3^-. We have noted this reaction in the preparation of many other actinide and transition metal iodates.[40,48] The use of the AIO_4 (A = NH_4, K, Rb, Cs) starting materials allows us to have more control over reaction pH and to avoid contamination with other anions than if alkali metal halides or other salts were used in these reactions.

When V_2O_5 is reacted with KIO_4 and I_2O_5 in a 1:2:1 ratio, **1** is the sole product obtained. Substantial variations in starting material stoichiometry have not allowed for the isolation of other potassium-containing products. When the size of cation is increased from K^+ (1.65 Å) to Rb^+ (1.75 Å), a mixture of both **2** and **4** is obtained when the V_2O_5:$RbIO_4$:I_2O_5 ratio is 1:1:1, but when this ratio is changed to 1:2:1, pure **2** is isolated. In the synthesis of **3**, we observed that when the ratio of V_2O_5:NH_4IO_4:I_2O_5 was held at 1:1:1 that both $VO_2(IO_3)\cdot 2H_2O$[41] and **3** were obtained, but that by increasing the ratio to 1:2:1 that pure **3** was formed. Pure **4** could not be obtained through a similar procedure. Finally, when Cs^+ (1.90 Å) is employed as the cation,[49] only **5** is isolated. It is interesting that when cations with ionic radii of ≈2 Å are used that $A[(VO)_2(IO_3)_3O_2]$ (A = NH_4 (**3**) or Cs (**5**)) are obtained, but when smaller cations are incorporated, $A[VO_2(IO_3)_2]$ (A = K (**1**)) is isolated. The Rb^+ cation, being of intermediate size, allows for the isolation of both types of compounds.

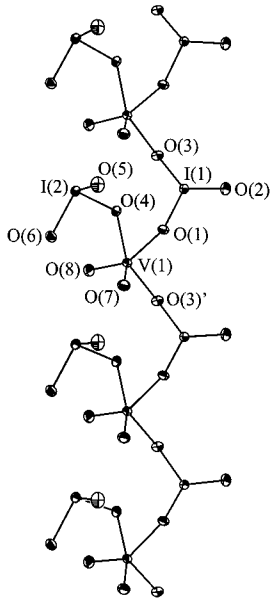

Figure 1. One-dimensional $^1_\infty[VO_2(IO_3)_2]^{1-}$ chains separated by K^+ or Rb^+ cations in $A[VO_2(IO_3)_2]$ (A = K (**1**), Rb (**2**)). 50% thermal ellipsoids are depicted.

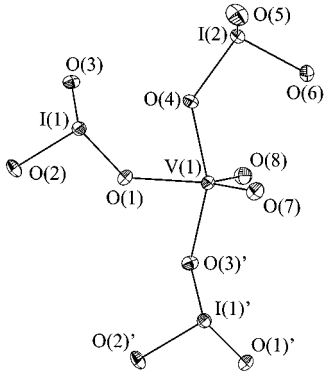

Figure 2. The fundamental building unit in $A[VO_2(IO_3)_2]$ (A = K (**1**), Rb (**2**)). These distorted square pyramidal V(V) centers are bound by two terminal oxo atoms to create a *cis*-VO_2^+ moiety and by one monodentate and two bridging iodate anions. 50% thermal ellipsoids are depicted.

There are additional structural factors associated with these cations that influence the type of products that can be isolated that will be discussed in the following sections.

Structures. *$K[VO_2(IO_3)_2]$ (**1**) and $Rb[VO_2(IO_3)_2]$ (**2**).* The structures of **1** and **2** both contain one-dimensional $^1_\infty[VO_2(IO_3)_2]^{1-}$ chains separated by K^+ or Rb^+ cations as depicted in Figure 1. In **1**, the chains run down the *b*-axis, whereas in **2**, the chains are along the *a*-axis. These chains are constructed from five-coordinate V(V) atoms that are bound by two terminal oxo atoms to create a *cis*-VO_2^+ moiety and by one monodentate and two bridging iodate anions to create a distorted square pyramidal geometry, which is shown in Figure 2. The two bridging iodate anions occupy adjacent corners on the base of the square pyramid. The vanadyl, V=O, moieties are easily identified by their short V−O bond distances that are 1.625(4) and 1.642(4) Å in **1** and 1.628(5) and 1.634(5) Å in **2**. There is little variation between the V−O bond distances associated with the bridging iodate anions versus the terminal ones. These bond distances range from 1.978(4) to 2.017(4) Å for **1**

(48) Bean, A. C.; Peper, S. M.; Albrecht-Schmitt, T. E. *Chem. Mater.* **2001**, *13*, 1266.
(49) (a) Shannon, R. D. *Acta Crystallogr.* **1976**, *A32*, 751. (b) Shannon, R. D.; Prewitt, C. T. *Acta Crystallogr.* **1969**, *B25* 925.

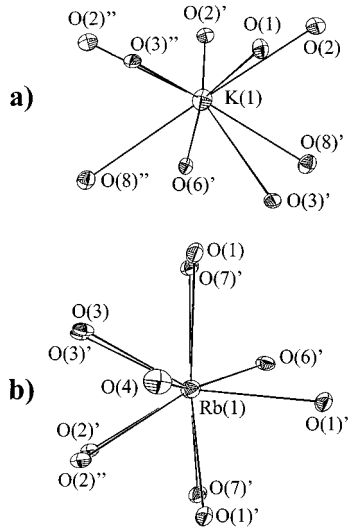

Figure 3. (a) The nine-coordinate local environment of the K^+ cations in $K[VO_2(IO_3)_2]$ (**1**). This geometry is best described as a capped square prism. (b) The Rb^+ cations in $Rb[VO_2(IO_3)_2]$ (**2**) form 11 contacts with surrounding oxygen atoms to create a capped pentagonal prism. 50% thermal ellipsoids are depicted.

and from 1.968(4) to 2.044(4) Å for **2**. The bond valence sums for the vanadium centers in **1** and **2** are 4.96 and 4.94, respectively.[50,51]

On the basis of the structures of other iodate compounds, we would anticipate that the I−O bond lengths for oxygen atoms bound to the vanadium centers to be longer than the terminal oxo groups.[40,48] This correlation is also found in the structures of **1** and **2**. For example, in **2** the two terminal oxo units of the monodentate iodate anion have I−O bond distances of 1.808(4) and 1.802(5) Å, while the oxygen atom coordinated to the V(V) center has a I−O bond distance of 1.847(4) Å. The same situation is also observed in the I−O bond distances for the bridging iodate anion where the shortest distance of 1.776(4) Å is to the terminal oxygen atom, whereas the bridging oxygen atoms display considerably longer I−O bond lengths of 1.820(4) and 1.841(4) Å. A similar scenario is found for the I−O bond distances in **1**.

The primary difference between the structures of **1** and **2** is the nature of the coordination of the alkali metal cations. The K^+ cations in **1** reside in nine-coordinate monocapped square prismatic sites with long $K^+\cdots O$ contacts ranging from 2.776(4) to 3.354(4) Å. In contrast, the Rb^+ cations present in **2** are 11-coordinate and occur in a geometry that is best described as a monocapped pentagonal prism. The local environments of these cations are shown in Figure 3a,b. Illustrations of the packing of the anionic one-dimensional chains and alkali metal cations in **1** and **2** are shown in Figures 4 and 5, respectively. Selected bond distances and angles for **1** and **2** are given in Tables 2 and 3, respectively.

*$A[(VO)_2(IO_3)_3O_2]$ ($A = NH_4$ (**3**), Rb (**4**), Cs (**5**)).* The architectural features of the isostructural series of **3**−**5**, while still one-dimensional, are quite distinct from that of **1** and **2**. First, the V(V) centers occur as orthorhombically (C_2) distorted VO_6 octahedra instead of as VO_5 distorted square pyramids. Second, a single terminal oxo group coordinates the vanadium atoms, and a *cis*-VO_2^+ unit is not present. Third, the bridging of vanadium polyhedra is accomplished through both additional oxo groups and by three iodate anions. Finally, the iodate anions in **3**−**5** only occur as bridging ligands. The

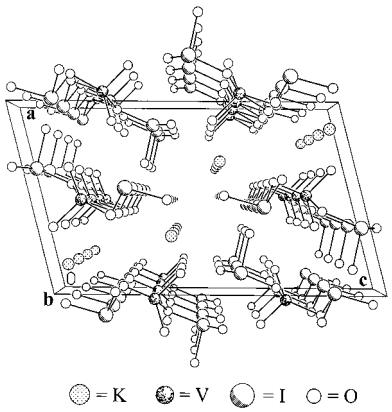

Figure 4. Part of the structure of $K[VO_2(IO_3)_2]$ (**1**) showing the packing of the one-dimensional $^1_\infty[VO_2(IO_3)_2]^{1-}$ chains with the K^+ cations.

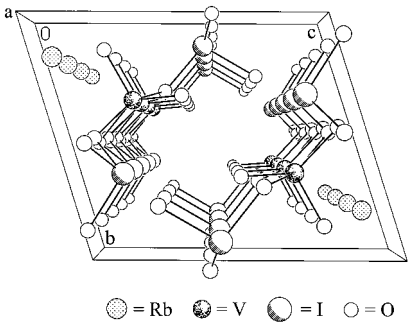

Figure 5. A view of the structure of $Rb[VO_2(IO_3)_2]$ (**2**) showing the packing of the one-dimensional $^1_\infty[VO_2(IO_3)_2]^{1-}$ chains with the Rb^+ cations.

Table 2. Selected Bond Distances (Å) and Angles (deg) for $K[VO_2(IO_3)_2]$ (1)

V(1)−O(1)	2.017(4)	I(1)−O(2)	1.771(4)
V(1)−O(3)	1.978(4)	I(1)−O(3)	1.834(4)
V(1)−O(4)	1.985(4)	I(2)−O(4)	1.853(4)
V(1)−O(7) (V=O)	1.642(4)	I(2)−O(5)	1.788(4)
V(1)−O(8) (V=O)	1.625(4)	I(2)−O(6)	1.803(4)
I(1)−O(1)	1.831(4)		
Bond Angles (deg) for the VO_5 Distorted Square Pyramid			
O(1)−V(1)−O(3)′	79.9(2)	O(3)′−V(1)−O(7)	96.9(2)
O(1)−V(1)−O(4)	76.6(2)	O(3)′−V(1)−O(8)	97.1(2)
O(1)−V(1)−O(7)	137.9(2)	O(4)−V(1)−O(7)	94.8(2)
O(1)−V(1)−O(8)	114.7(2)	O(4)−V(1)−O(8)	100.4(2)
O(3)′−V(1)−O(4)	155.0(2)	O(7)−V(1)-O(8)	107.3(2)

Table 3. Selected Bond Distances (Å) for $Rb[VO_2(IO_3)_2]$ (2)

V(1)−O(2)	1.968(4)	I(1)−O(2)	1.841(4)
V(1)−O(3)	2.044(4)	I(1)−O(3)	1.820(4)
V(1)−O(5)	1.994(4)	I(2)−O(4)	1.802(5)
V(1)−O(7) (V=O)	1.628(5)	I(2)−O(5)	1.847(4)
V(1)−O(8) (V=O)	1.634(5)	I(2)−O(6)	1.808(4)
I(1)−O(1)	1.776(4)		
Bond Angles (deg) for the VO_5 Distorted Square Pyramid			
O(2)−V(1)−O(3)	81.2(2)	O(3)−V(1)−O(7)	109.3(2)
O(2)−V(1)−O(5)′	154.2(2)	O(3)′−V(1)−O(8)	143.3(2)
O(2)−V(1)−O(7)	98.4(2)	O(5)′−V(1)−O(7)	100.4(2)
O(2)−V(1)−O(8)	97.0(2)	O(5)′−V(1)−O(8)	94.2(2)
O(3)′−V(1)−O(5)′	75.9(2)	O(7)−V(1)−O(8)	107.2(3)

(50) Brown, I. D.; Altermatt, D. *Acta Crystallogr.* **1985**, *B41*, 244.
(51) Brese, N. E.; O'Keeffe, M. *Acta Crystallogr.* **1991**, *B47*, 192.

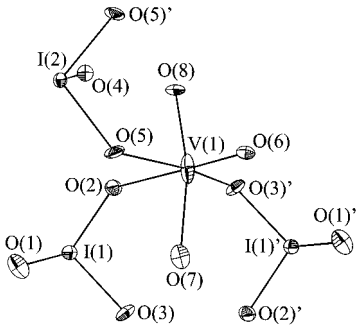

Figure 6. A depiction of the fundamental building unit in $NH_4[(VO)_2(IO_3)_3O_2]$ (**3**), $Rb[(VO)_2(IO_3)_3O_2]$ (**4**), and $Cs[(VO)_2(IO_3)_3O_2]$ (**5**) showing the orthorhombically distorted VO_6 octahedron formed from one terminal and two bridging oxo groups and three bridging iodate anions. 50% thermal ellipsoids are depicted.

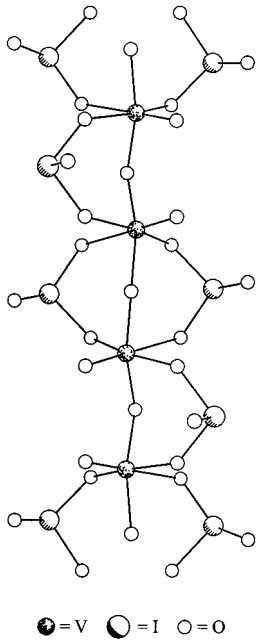

Figure 7. The zigzagging one-dimensional $^1_\infty[(VO)_2(IO_3)_3O_2]^{1-}$ chains in $NH_4[(VO)_2(IO_3)_3O_2]$ (**3**), $Rb[(VO)_2(IO_3)_3O_2]$ (**4**), and $Cs[(VO)_2(IO_3)_3O_2]$ (**5**) that are separated from one another by NH_4^+, Rb^+, or Cs^+ cations.

fundamental structural building unit for these compounds is shown in Figure 6. The bridging oxo atoms are trans to one another, and the three bridging iodate anions are in a mer arrangement. This creates zigzagging one-dimensional $^1_\infty[(VO)_2(IO_3)_3O_2]^{1-}$ chains that are separated from one another by NH_4^+, Rb^+, or Cs^+ cations. These chains can also be viewed as being constructed from corner-sharing VO_6 octahedra and are shown in Figure 7. When viewed down the *a*-axis, which is the direction of chain propagation, the structure almost appears to be three-dimensional (Figure 8). This is because the iodate anions from each chain are interdigitated with one another. Therefore, these chains are more tightly packed than those observed in **1** or **2**.

The vanadyl moiety is easily identified by the short V═O bond distance which has an average bond distance of 1.619(9) Å in **3**−**5**. This distance is considerably shorter than, and easily distinguished from, the V(V)−O(H_2O) distance of 2.039(3) Å in $VO_2IO_3{\cdot}2H_2O$.[41] V−O bonds of intermediate length are formed with the

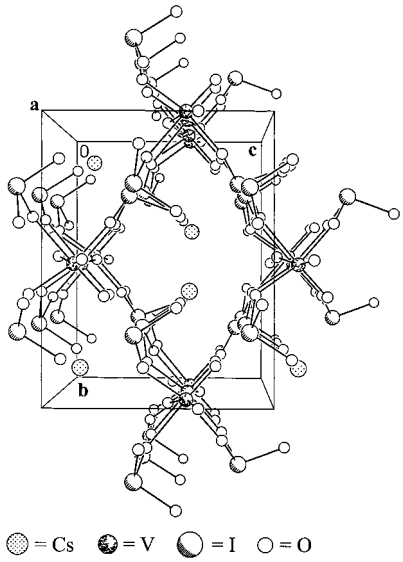

Figure 8. An illustration of the packing of the one-dimensional $^1_\infty[(VO)_2(IO_3)_3O_2]^{1-}$ anionic chains with the Cs^+ cations in $Cs[(VO)_2(IO_3)_3O_2]$ (**5**). This figure also shows a view of the alignment of the stereochemically active lone pairs of electrons of the iodate anions along the *c*-axis that create the polarity in the structures.

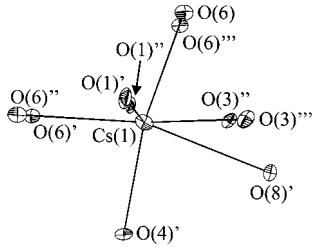

Figure 9. A depiction of the Cs^+ cations in $Cs[(VO)_2(IO_3)_3O_2]$ (**5**) that occur in irregular 10-coordinate environments. 50% thermal ellipsoids are depicted.

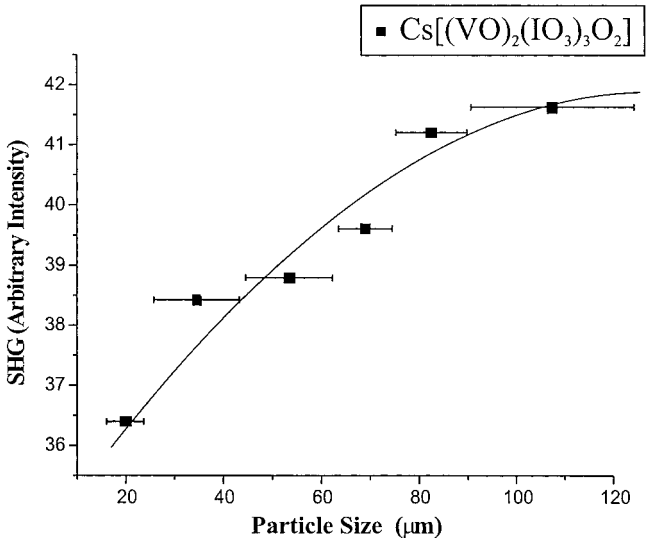

Figure 10. Phase-matching curve (Type 1) for $Cs[(VO)_2(IO_3)_3O_2]$ (**5**). The curve is to guide the eye and is not a fit to the data.

bridging oxo atoms. These bonds range from 1.867(7) to 1.886(4) Å in **3**−**5**. The remaining three V−O bonds are formed with the bridging iodate anions. These bonds are notably longer than the vanadium−oxo bond distances and occur from 1.989(8) to 2.227(8) Å in **3**−**5**.

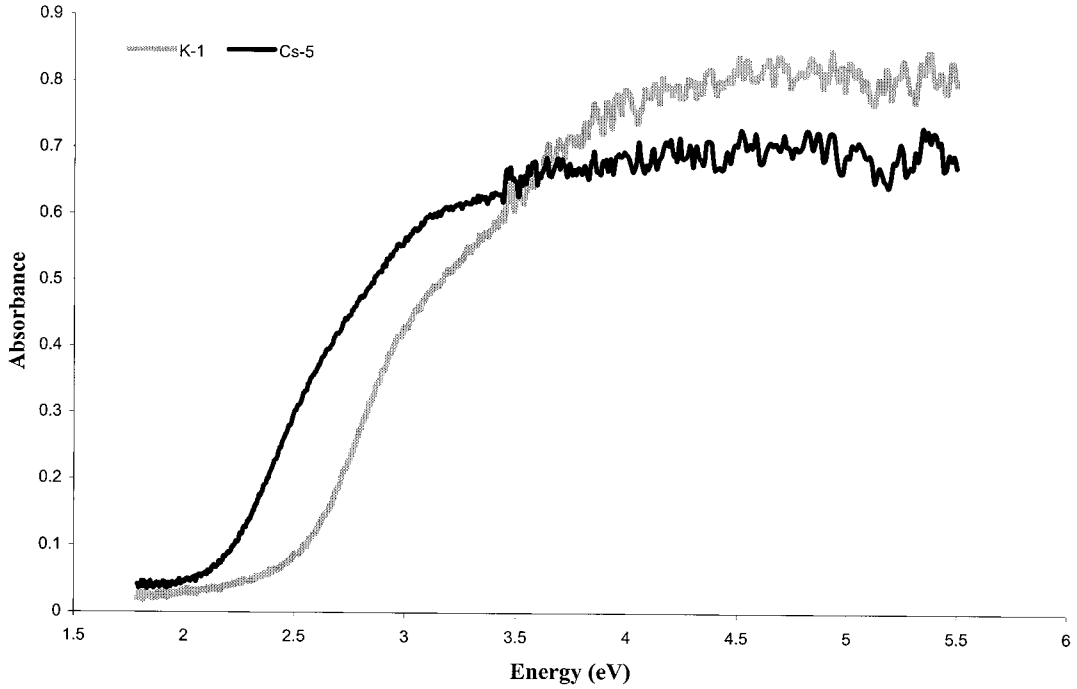

Figure 11. UV−vis diffuse reflectance spectra of $K[VO_2(IO_3)_2]$ (**1**) and $Cs[(VO)_2(IO_3)_3O_2]$ (**5**).

Table 4. Selected Bond Distances (Å) for $NH_4[(VO)_2(IO_3)_3O_2]$ (3)

V(1)−O(2)	2.227(8)	I(1)−O(1)	1.794(9)
V(1)−O(3)′	1.950(8)	I(1)−O(2)	1.818(9)
V(1)−O(5)	1.989(8)	I(1)−O(3)	1.848(8)
V(1)−O(6) (V=O)	1.620(9)	I(2)−O(4)	1.77(1)
V(1)−O(7)	1.878(4)	I(2)−O(5)	1.833(8)
V(1)−O(8)	1.873(6)	I(2)−O(5)′	1.833(8)

Bond Angles (deg) for the VO_6 Distorted Octahedron

O(2)−V(1)−O(3)′	82.1(3)	O(3)′−V(1)−O(8)	88.7(5)
O(2)−V(1)−O(5)	82.8(3)	O(5)−V(1)−O(6)	96.2(4)
O(2)−V(1)−O(6)	178.8(4)	O(5)−V(1)−O(7)	86.0(4)
O(2)−V(1)−O(7)	83.7(3)	O(5)−V(1)−O(8)	89.4(5)
O(2)−V(1)−O(8)	80.5(4)	O(6)−V(1)−O(7)	97.1(4)
O(3)′−V(1)−O(5)	165.0(4)	O(6)−V(1)−O(8)	98.7(5)
O(3)′−V(1)−O(6)	98.8(4)	O(7)−V(1)−O(8)	164.0(4)
O(3)′−V(1)−O(7)	91.7(4)		

Table 5. Selected Bond Distances (Å) for $Rb[(VO)_2(IO_3)_3O_2]$ (4)

V(1)−O(2)	2.20(1)	I(1)−O(1)	1.78(1)
V(1)−O(3)′	1.94(1)	I(1)−O(2)	1.83(1)
V(1)−O(5)	2.00(1)	I(1)−O(3)	1.85(1)
V(1)−O(6) (V=O)	1.62(1)	I(2)−O(4)	1.80(2)
V(1)−O(7)	1.872(6)	I(2)−O(5)	1.84(1)
V(1)−O(8)	1.867(7)	I(2)−O(5)′	1.84(1)

Bond Angles (deg) for the VO_6 Distorted Octahedron

O(2)−V(1)−O(3)′	83.1(5)	O(3)′−V(1)−O(8)	89.8(5)
O(2)−V(1)−O(5)	82.8(3)	O(5)−V(1)−O(6)	95.0(5)
O(2)−V(1)−O(6)	177.8(6)	O(5)−V(1)−O(7)	86.4(5)
O(2)−V(1)−O(7)	82.6(5)	O(5)−V(1)−O(8)	89.0(5)
O(2)−V(1)−O(8)	81.0(5)	O(6)−V(1)−O(7)	97.3(6)
O(3)′−V(1)−O(5)	165.9(5)	O(6)−V(1)−O(8)	99.1(6)
O(3)′−V(1)−O(6)	99.1(5)	O(7)−V(1)−O(8)	163.3(5)
O(3)′−V(1)−O(7)	90.8(6)		

Therefore, these compounds do not display the commonly observed 2 + 2 + 2 bonding scheme that is found in compounds that contain two terminal oxo groups, such as octahedral Mo(VI) compounds where there are two short, two intermediate, and two long Mo−O bond distances.[52] Much like the Mo(VI) centers in $AMoO_3(IO_3)$ (A = K, Rb, Cs),[40] the V(V) atoms do show evidence of a significant second-order Jahn−Teller distortion[31−39] that shifts the metal centers ≈0.27 Å along the C_2 axis of the VO_6 octahedra. The bond valence sums for the vanadium atoms in **3**−**5** are 4.88, 4.93, and 4.87, respectively.

Table 6. Selected Bond Distances (Å) for $Cs[(VO)_2(IO_3)_3O_2]$ (5)

V(1)−O(2)	2.215(8)	I(1)−O(1)	1.770(8)
V(1)−O(3)′	1.941(8)	I(1)−O(2)	1.836(8)
V(1)−O(5)	1.996(8)	I(1)−O(3)	1.866(7)
V(1)−O(6) (V=O)	1.620(8)	I(2)−O(4)	1.82(1)
V(1)−O(7)	1.886(4)	I(2)−O(5)	1.839(8)
V(1)−O(8)	1.875(5)	I(2)−O(5)′	1.839(8)

Bond Angles (deg) for the VO_6 Distorted Octahedron

O(2)−V(1)−O(3)′	82.6(4)	O(3)′−V(1)−O(8)	88.7(4)
O(2)−V(1)−O(5)	83.4(3)	O(5)−V(1)−O(6)	94.6(4)
O(2)−V(1)−O(6)	178.0(4)	O(5)−V(1)−O(7)	86.7(3)
O(2)−V(1)−O(7)	84.5(3)	O(5)−V(1)−O(8)	89.1(4)
O(2)−V(1)−O(8)	80.5(4)	O(6)−V(1)−O(7)	95.7(4)
O(3)′−V(1)−O(5)	166.0(4)	O(6)−V(1)−O(8)	99.2(4)
O(3)′−V(1)−O(6)	99.4(4)	O(7)−V(1)−O(8)	164.8(4)
O(3)′−V(1)−O(7)	91.9(4)		

As found for **1** and **2**, the I−O bond lengths show expected variations based on whether they coordinate the V(V) centers or if they are terminal. For example, in **5** the two terminal I−O bonds between I(1) and O(1) and between I(2) and O(4) at 1.770(8) and 1.82(1) Å are shorter than the remaining I−O bonds, all of which are bridged to vanadium atoms. These latter bond distances range from 1.836(8) to 1.866(7) Å and are typical for I−O bonds involved in coordination to high-valent metal

(52) Hagrman, P. J.; LaDuca, R. L., Jr.; Koo, H.-J.; Rarig, R., Jr.; Haushalter, R. C.; Whangbo, M.-H.; Zubieta, J. *Inorg. Chem.* **2000**, *39*, 4311.

centers.[40,48] Selected bond distances and angles for **3**−**5** are given in Tables 4−6, respectively.

The NH_4^+, Rb^+, or Cs^+ cations in **3**−**5** are present on 4b mirror sites. The Rb^+ and Cs^+ cations in **4** and **5** occur in irregular 10-coordinate environments. While the hydrogen atoms on the NH_4^+ cation could not be located, the fact that the nitrogen atom is on a mirror plane and that there is a short N···O contact of ≈2.8 Å implies that there is hydrogen bonding present and that the protons are likely to be ordered. The geometry around the Rb^+ and Cs^+ cations in **4** and **5** are much less regular than that of the K^+ and Rb^+ cations in **1** and **2**. The local environment of the Cs^+ cations in **5** is depicted in Figure 9.

The final and most important feature of these compounds is that they crystallize in the polar space group *Ima*2. The polarity in these structures is imparted by the alignment of the stereochemically active lone pairs of electrons of the iodate anions along the *c*-axis as is shown in Figure 8. It should be noted that the iodate anions in the one-dimensional chains in $VO_2IO_3 \cdot 2H_2O$ also align in one direction.[41] However, this structure is centrosymmetric and crystallizes in the monoclinic space group $P2_1/c$. Therefore, while an individual chain is polar, the chains pack in two opposite orientations in the structure to yield a structure without polarity.

Nonlinear Optical Properties. In the absence of an external physical property measurement that confirms acentricity, it can be haphazard to refine a structure in a noncentrosymmetric setting.[53,54] While we were unable to solve the structures of **3**−**5** in a centrosymmetric space group, it is still possible that their space group is incorrect. Second-harmonic generation (SHG) measurements allow for confirmation of our space group assignment and provide an evaluation of the potential usefulness of these compounds in device applications. SHG measurements were performed using a modified Kurtz-NLO system with a 1064-nm light source on powders ground from crystals of **5**. Compound **5** was chosen as a representative of the group because of the ease in which its synthesis can be scaled up to yield gram quantities of high-purity crystalline product. Generation of SHG light of 532 nm was carefully measured, and these studies indicated a large response for **5** of 500× α-quartz. The birefringence of **5** is significant enough for phase matchability (Type 1) as shown in Figure 10. Calculations using methods described earlier[44,55] give an average NLO susceptibility, $\langle d_{ijk}^{2\omega} \rangle$ or $\langle d_{\text{eff}} \rangle$, of 26 pm/V. The large response of **5** is due to not only the polarity of the space group and the alignment of the lone pairs on the iodate anions but also the large degree of polarization of the V(V)−O bonds.

UV−**Vis Diffuse Reflectance Spectra.** Compounds **1**−**5** all contain pentavalent vanadium and therefore lack d electrons that would yield the intense green and blue colorations found with V(IV)/V(V) and V(IV) systems. Therefore, the yellow to orange coloration observed from these compounds can probably be ascribed to charge transfer from the iodate anions to the highly electropositive V(V) centers. UV−vis diffuse reflectance spectra collected from **1** and **5** are consistent with this description and show the onset of absorption between 2 and 2.5 eV, as shown in Figure 11, which means they are absorbing light in approximately the green region of the EM spectrum. Compound **5** absorbs at lower eV than **1**, providing its orange coloration. Plots of absorbance^2 versus energy and absorbance$^{1/2}$ versus energy at the absorption edge both show nearly linear dependence with R^2 values of 0.99 and 0.99, respectively. Therefore, it is unclear whether these compounds have direct or indirect band gaps.[56,57]

Conclusions

In a seminal paper by Kurtz and co-workers it was established that the successful preparation of new nonlinear optical materials was often dependent on the combination of three key structural features.[58] First, anions with a nonbonding, but stereochemically active, pair of electrons such as selenite[59−63] or iodate[64−73] have a tendency to align in the solid state to create polar structures. Second, d^0 transition metals were already recognized as being susceptible to distortion from idealized octahedral symmetry, that is, a second-order Jahn−Teller distortion (vide supra). These distortions can be cooperative and lead to noncentrosymmetric (NCS) structures. Finally, large cations such as Ba^{2+} and Cs^+ have a propensity for residing in sites where they form contacts with eight or more anions in an acentric environment. Smaller cations such as K^+, on the other hand, are often present in more symmetric environments. Therefore, the culmination of these three concepts would be to prepare compounds containing large cations, d^0 transition metals, and anions with a nonbonding pair of electrons. While there is no guarantee

(53) Marsh, R. E. *Acta Crystallogr.* **1992**, *B48*, 356.
(54) Ermer, O.; Dunitz, J. *Acta Crystallogr.* **1970**, *A26*, 163.
(55) Ok, K. M.; Bhuvanesh, N. S. P.; Halasyamani, P. S. *J. Solid State Chem.* **2001**, *161*, 57.
(56) Pankove, J. I. *Optical Processes in Semiconductors*; Prentice Hall, Inc.: Engelwood Cliffs, NJ, 1971.
(57) Feger, C. R.; Kolis, J. W.; Gorny, K.; Pennington, C. *J. Solid State Chem.* **1999**, *143*, 254.
(58) Bergman, J. G., Jr.; Boyd, G. D.; Ashkin, A.; Kurtz, S. K. *J. Appl. Phys.* **1969**, *70*, 2860.
(59) Kwon, Y.-U.; Lee, K.-S.; Kim, Y. H. *Inorg. Chem.* **1996**, *35*, 1161.
(60) Vaughey, J. T.; Harrison, W. T. A.; Dussack, L. L.; Jacobson, A. J. *Inorg. Chem.* **1994**, *33*, 4370.
(61) Harrison, W. T. A.; Dussack, L. L.; Jacobson, A. J. *J. Solid State Chem.* **1996**, *125*, 234.
(62) Harrison, W. T. A.; Dussack, L. L.; Jacobson, A. J. *Inorg. Chem.* **1994**, *33*, 6043.
(63) Dussack, L. L.; Harrison, W. T. A.; Jacobson, A. J. *Mater. Res. Bull.* **1996**, *31*, 249.
(64) Svenson, C.; Abrahams, S. C.; Bernstein, J. L. *J. Solid State Chem.* **1981**, *36*, 195.
(65) Nassau, K.; Shiever, J. W.; Prescott, B. E. *J. Solid State Chem.* **1973**, *7*, 186.
(66) Nassau, K.; Shiever, J. W.; Prescott, B. E. *J. Solid State Chem.* **1973**, *8*, 260.
(67) Nassau, K.; Shiever, J. W.; Prescott, B. E.; Cooper, A. S. *J. Solid State Chem.* **1974**, *11*, 314.
(68) Liminga, R.; Abrahams, S. C.; Bernstein, J. L. *J. Chem. Phys.* **1975**, *62*, 755.
(69) Nassau, K.; Shiever, J. W.; Prescott, B. E. *J. Solid State Chem.* **1975**, *14*, 122.
(70) Abrahams, S. C.; Bernstein, J. L.; Nassau, K. *J. Solid State Chem.* **1976**, *16*, 173.
(71) Abrahams, S. C.; Bernstein, J. L.; Nassau, K. *J. Solid State Chem.* **1977**, *22*, 243.
(72) Liminga, R.; Abrahams, S. C.; Bernstein, J. L. *J. Chem. Phys.* **1977**, *67*, 1015.
(73) Gupta, P. K. S.; Ammon, H. L.; Abrahams, S. C. *Acta Crystallogr.* **1989**, *C45*, 175.

that the combination of these features will yield NCS structures, the tendency for this to be true is certainly apparent from extensive reviews of this area.[74] These ideas have been successfully applied in the syntheses of a number of NCS compounds including $AVSeO_5$ (A = Rb, Cs),[59] $A(VO)_3(SeO_3)_2$ (A = NH_4, K, Rb, Cs),[59,60] $A_2(MoO_3)_3SeO_3$ (A = NH_4, Rb, Cs, Tl),[60−63] and $AMoO_3(IO_3)$ (A = Rb, Cs).[40]

In this present study, we have demonstrated that these concepts hold true for alkali metal vanadium iodates and that Rb^+ represents the cusp between the structural transition from a centrosymmetric structure to a polar one. Here, subtle changes in reaction stoichiometry allow for the isolation of $Rb[VO_2(IO_3)_2]$ (**2**), which is centrosymmetric, and/or $Rb[(VO)_2(IO_3)_3O_2]$ (**4**), which is polar. The larger NH_4^+ and Cs^+ cations only allow for the production of $NH_4[(VO)_2(IO_3)_3O_2]$ (**3**) and $Cs[(VO)_2(IO_3)_3O_2]$ (**5**). The ammonium salt actually demonstrates yet another strategy put forward by Kurtz and co-workers for obtaining NCS structures because the tetrahedral geometry prohibits the nitrogen atom from residing on an inversion center without disordering on the protons.[58] It is therefore more likely that ammonium and other tetrahedral atoms will be located on mirror planes or general positions.[58,74]

Acknowledgment. TEA-S acknowledges NASA (ASGC) and the Department of Energy, Heavy Elements Program (Grant DE-FG02-01ER15187), for partial support of this work. P.S.H. acknowledges the Robert A. Welch Foundation for support. This work used the MRSEC/TCSUH Shared Experimental Facilities supported by the National Science Foundation under Award DMR-9632667 and the Texas Center for Superconductivity at the University of Houston. This work was also supported by the NSF-Career Program through DMR-0092054. An acknowledgment is made to the donors of the Petroleum Research Fund, administered by the American Chemical Society, for partial support of this research (TEA-S and P.S.H.).

Supporting Information Available: X-ray crystallographic files for $K[VO_2(IO_3)_2]$ (**1**), $Rb[VO_2(IO_3)_2]$ (**2**), $NH_4[(VO)_2(IO_3)_3O_2]$ (**3**), $Rb[(VO)_2(IO_3)_3O_2]$ (**4**), and $Cs[(VO)_2(IO_3)_3O_2]$ (**5**) (CIF). This material is available free of charge via the Internet at http://pubs.acs.org.

CM020021N

(74) Halasyamani, P. S.; Poeppelmeier, K. R. *Chem. Mater.* **1998**, *10*, 2753.